Received: 25 June 2018 | Revised: 17 November 2019 | Accepted: 24 January 2020

DOI: 10.1111/jfr3.12599

ORIGINAL ARTICLE

CIWEM Chartered Institution of Water and Environmental Management | Journal of Flood Risk Management | WILEY

Bridge pier shape influence on wood accumulation: Outcomes from flume experiments and numerical modelling

Pina N. De Cicco[1] | **Enio Paris**[1] | **Luca Solari**[1] | **Virginia Ruiz-Villanueva**[2]

[1]Department of Civil and Environmental Engineering, University of Florence, Florence, Italy

[2]Department of Earth Sciences, University of Geneva, Geneva, Switzerland

Correspondence
Luca Solari, Professor, Department of Civil and Environmental Engineering, University of Florence, Florence, Italy.
Email: luca.solari@unifi.it

Abstract

Streamwood accumulation at bridges exerts additional forces to bridge structures and may aggravate flooding, local scouring, and eventually may lead to bridge collapse. However, the important ecological role of streamwood in fluvial systems calls for a compromise between preservation of river ecosystems and prevention of streamwood-related hazards (e.g., bridge clogging). This study evaluates the effect of bridge pier shape on wood accumulation or blockage, probability in lowland type of rivers. We conducted laboratory experiments in a flume testing various pier shapes and wood transport mechanisms under two different flow conditions, complemented with numerical modelling. Results revealed that the flow field immediately upstream from the pier has a significant influence on the blockage probability. The pier shape is controlling the flow field, thus, it has a significant influence on wood accumulation. In particular, a squared pier shape, higher Froude number and semi-congested wood transport resulted in the highest blockage probability under the tested conditions. Our results may help to better design infrastructures to mitigate streamwood-related hazards in rivers.

KEYWORDS

blockage probability, bridge clogging, streamwood, wood accumulation

1 | INTRODUCTION

Streamwood is usually referred to logs longer than 1 m with a diameter of 0.1 m transported by flow (Wohl et al., 2010). Instream large wood enters rivers by different recruitment processes along the fluvial corridor or from the hillslopes (e.g., bank erosion, landslides, and other types of mass movements; Benda & Sias, 2003). The presence of streamwood in rivers provides habitat diversity and nutriment for invertebrates, fishes, and other vertebrates (Benke & Wallace, 2003; Harmon, Franklin, & Swanson, 1986). Natural wood accumulations (i.e., jams) create storage areas for organic material; this, together with the decomposition of wood itself, provides a rich nutrient source for aquatic species, and a functional component of fluvial ecosystems (see, e.g., Gurnell, 2013; Le Lay, Piégay, & Moulin, 2013; Ruiz-Villanueva, Piégay, Gurnell, Marston, & Stoffel, 2016; Solari, Van Oorschot, Hendriks, Rinaldi, & Vargas-Luna, 2015). Importantly, due to the natural afforestation in many European

catchments because of the abandonment of agricultural lands occurred in the last decades, the presence of wood in rivers has generally increased (e.g., Comiti, 2012). Moreover, wood is reintroduced in altered river systems as a restoration measure (Kail, Hering, Muhar, Gerhard, & Preis, 2007). This increase in streamwood storage may have positive effects on the fluvial ecosystems, but under certain circumstances (e.g., urbanised areas) the transport of large quantities of wood during floods may imply hazards for humans and infrastructures. This is particularly important at critical sections such as bridges, where wood accumulation may produce significant damages.

Wood accumulation at bridge piers has been identified as one of the most frequent causes of bridge failures in the Unites States (Diehl, 1997), and many damages to infrastructures were observed during several recent flood events in Europe (e.g., the 2011 flood in the Magra river basin in north-western Italy and the central part of the country in 2005 or the Emme catchment in Switzerland in 2014; Badoux et al., 2015; Comiti, Lucía, & Rickenmann, 2016; Steeb, Rickenmann, Badoux, Rickli, & Waldner, 2017).

Wood accumulation at bridges may reduce the effective flow area thereby decreasing the river conveyance, producing a backwater effect, which may intensify flooding (Okamoto, Takebayashi, Sanjou, Suzuki, & Toda, 2019). It can also lead to bridge failure due to both additional hydrodynamic forces generated in proximity of the wood accumulation (Manners, Doyle, & Small, 2007; Parola, Apelt, & Jempson, 2000) and increase of local scouring (Kattell & Eriksson, 1998).

Previous flume experiments carried out on the interaction between wood and bridges emphasise the most favourable bridge deck for wood transit or the effects of clogging caused by in-channel wood on the water level and a mobile bed profile (Melville & Dongol, 1992; Pagliara & Carnacina, 2011; Schalko, Schmocker, Weitbrecht, & Boes, 2016; Schmocker & Hager, 2011). Previous investigations on wood accumulation at a single pier aimed to study the effect of wood blockage on flow velocity and water depth, or the correlation between the shape of the wood accumulation and the resulted scour or the blockage probability in the presence of a pier (Gschnitzer, Gems, Aufleger, Mazzorana, & Comiti, 2013; Lagasse, Clopper, Zevenbergen, Spitz, & Girard, 2010; Lyn, Cooper, Yi, Sinha, & Rao, 2003). The experimental analysis on wood accumulation at a square pier with rounded nose and the field monitoring at bridges with video recording by Lyn et al. (2003) and Lyn, Cooper, Condon, and Gan (2007) proved that (a) smaller velocity and flow depth favour the accumulation of wood at bridges (in case of rounded pier shape); (b) in-channel wood delivery tends to be more like a succession of impulses than a continuous release; and that (c) the in-channel wood is more prone to stop at the pier located within the channel than close to the banks. Schmocker and Hager (2011) analysed the wood blocking probability of single logs and rootwads of different dimensions, under different freeboard and flow conditions and for different bridge deck geometries. These authors derived blocking probability equations based on the analysed variables and identified freeboard and wood dimensions as the most relevant. Latter works by Gschnitzer et al. (2013) and Gschnitzer, Gems, Mazzorana, and Aufleger (2017) evaluated the bridge obstruction caused by wood with and without a central semicircular pier and proposed a logistic regression model based on hydraulic parameter and wood characteristics. However, the general application of those equations is limited to the ranges of the conditions under which they were derived.

While these studies focused on wood accumulation at bridges, they neglected additional aspects concerning the hydraulics of the problem (De Cicco, Paris, Ruiz-Villanueva, Solari, & Stoffel, 2018). In particular, the flow field around the structure, which is determined by the pier shape, acts on the log motion thus affecting the blockage probability. Therefore, a better knowledge of wood accumulation at bridge piers is required to better develop flood mitigation strategies, such as improving bridge design to allow wood passage.

This work aims to fill this gap by investigating the effects of bridge pier shape on wood accumulation (De Cicco, Paris, & Solari, 2016 for some preliminary results). To do this, the main dimensionless parameters governing the pier blockage probability are described and the influence of these parameters is investigated through a hybrid approach combining laboratory experiments and 2D numerical modelling.

2 | METHODOLOGY

2.1 | Experimental design and measuring instruments

The experiments were done at the hydraulic laboratory of the Department of Civil and Environmental Engineering of the University of Firenze (Italy), in a glass-walled rectangular flume 5 m long, 0.30 m, wide and 0.16 m deep. The flume bed had a fixed slope of 0.001 which was covered by a layer of uniform gravel (D_{50} = 6.81 mm) glued on a fixed plate. The downstream water level was controlled by a sluice gate. The recirculating water flow into the flume was regulated by a valve and measured by means of an electromagnetic flowmeter (model Asamag,

flow range 0–14 L/s). The flow velocities were measured at six cross-sections upstream of the piers at a distance of 8 cm from the walls and at different depths utilising a STREAMFLO miniature current flowmeter system designed for measuring low velocities. The flow velocities in the range could be measured with an accuracy of ±2% of true velocity and maximum immersion length of 420 mm.

The water levels were recorded by means of three ultrasonic sensors Honeywell series 943- F4V-2D-1C0-330E. All the sensors recorded the water level with a frequency of 4 Hz and a maximum error of ±1 mm. Two sensors were fixed at the beginning and at the end of the channel, respectively, and one sensor was positioned upstream of the pier. The sensors measured the distance between the probe and the water surface along the centreline of the channel. The probes were connected to a PC with a data acquisition system and then the electronic signal was converted into a distance. The data recorded was transferred and process using the software LabView.

Figure 1 shows the side and top views of the flume and the position of the pier used in the experiments.

Two cameras were used during the tests to record the experiments. A Canon PowerShot camera, model SX600HS, was positioned at the beginning of the flume, for tracking the logs movement from the input point to the section in which the pier was positioned. A second camera, a Canon PowerShot model SX230HS, was fixed in correspondence of the pier in order to record the log accumulation formation and the logs entrapment at the pier.

2.2 | Scaling parameters

The present experiments were not set scaled from a specific prototype, but were designed to explore conditions occurring in a typical lowland river. Five pier geometries, three classes of logs, two wood transport mechanisms and two hydraulic conditions were performed under steady flow and fixed bed conditions. A total of 150 tests were realised. The following subsections describe all the scaling variables (for additional scaling issues, see also Supporting Information, A).

2.2.1 | The bridge piers

Five different pier shapes were built using a 3D printer with thermo-plastic material. The scaling of the piers was defined by the size of the flume and the ratio between pier width and pier length (without cutwater). Pier width ($w_p = 2.5$ cm) and length ($L_p = 7$ cm) were defined; the ratio $w_p/L_p = 0.36$ was kept constant which corresponds to common concrete bridges in European cities; for example, for the Margaret Bridge in Budapest ($w_p/L_p = 0.3$) and the Ponte Vecchio in Florence ($w_p/L_p = 0.34$). Values of w_p/L_p are reported in Table 1. Five cutwater shapes inspired in masonry bridges from historical European cities (e.g., the Ponte Vecchio in Florence, Wilson Bridge in Tours, and the Concorde Bridge in Paris; see also Section F in the Supporting Information) were reproduced (Figure 2).

The piers were glued to the flume bed in the middle of the cross-section at 3 m from the flume inlet and aligned with the flow.

2.2.2 | Wood modelling

To reproduce the wooden logs, beech wooden cylinders with no roots and no branches, were used. Importantly,

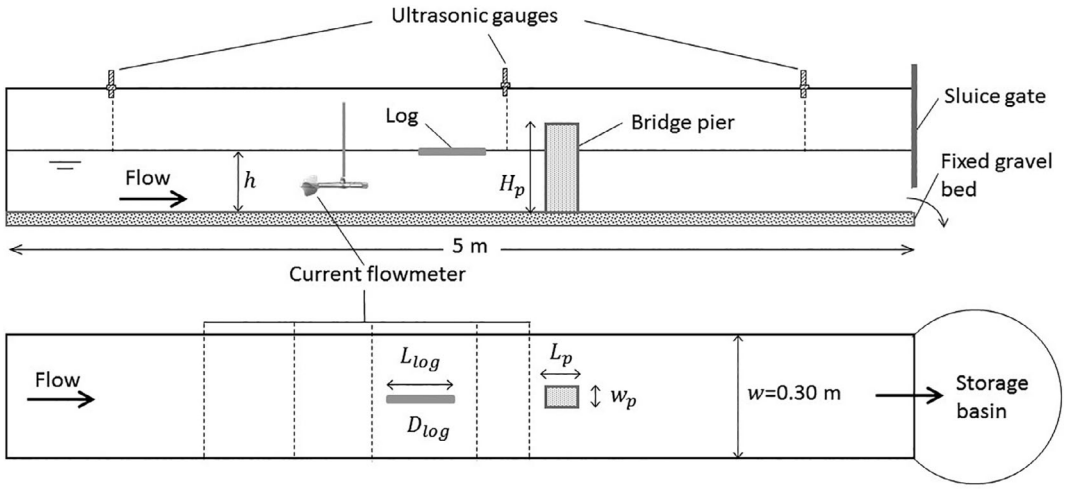

FIGURE 1 Side and top view of the laboratory flume

TABLE 1 Pier shapes reproduced in the laboratory

Code	Geometry	Figure	Similar example	(w_p/L_p)	$(w_p/L_p)_E$	$(w_p/L_p)_E/(w_p/L_p)$
R0	Square-nose		Tiberio Bridge (Rimini, Italy)	0.40	0.36	0.9
R1	Round-nose		Ponte Palatino (Rome, Italy)	0.38	0.36	0.95
R2	Triangular-nose (60°)		Ponte Vecchio (Florence, Italy)	0.34	0.36	1.06
R3	Ogival-nose		Wilson Bridge (Tours, France)	0.30	0.36	1.2
R4	Trapezoidal-nose		Dattaro Bridge (Parma, Italy)	0.33	0.36	1.09

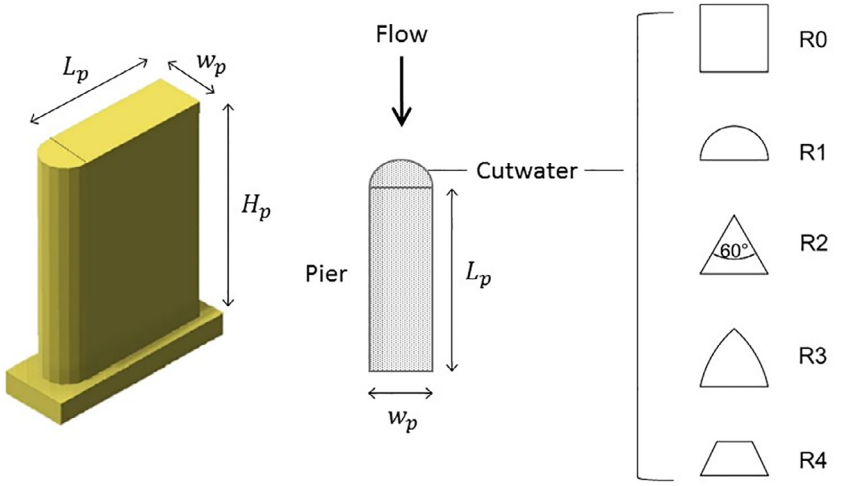

FIGURE 2 Bridge pier geometries reproduced in the laboratory (five cutwaters R0, R1, R2, R3, R4 were employed); (w_p/L_p) is the ratio pier width to its length for the example pier, $(w_p/L_p)_E$ is the adopted ratio in the experiments

this simple cylindrical geometry, represents a reasonable approximation of defoliated and non-rooted pieces of wood, commonly observed during fluvial transport in lowland rivers (Allen & Smith, 2012; Bocchiola, Rulli, & Rosso, 2008; Ruiz-Villanueva et al., 2014; Xu & Liu, 2016).

Three different log lengths (L_{log}) and diameters (D_{log}) were selected: small logs (length equal to the 20% of flume width, L_{log} = 6 cm and D_{log} = 0.2 cm), medium logs (length equal to the 30% of flume width, L_{log} = 9 cm and D_{log} = 0.4 cm) and large logs (length half of flume width, L_{log} = 15 cm and D_{log} = 0.6 cm), as reported in Table 2. A preliminary set of experiments (see Supporting Information, B) was carried out to determine the ratio between the log length and the flume width to avoid the 'log-walls' interactions (L_{log}/flume width ≤ 50%).

The relative proportion of each class of logs was defined to reproduce the typical properties and dimensions of wood in large lowland rivers, like the Arno River in Italy, the Indiana River in the United States (Manners et al., 2007), or the Slave River in Canada (Kramer & Wohl, 2014). According to field observations in these rivers, the ratio of small, medium and large wood was equivalent to 80:12:8% (Table 2). This ratio was used in the experiments as a reliable log size distribution in large lowland rivers, other log size distribution may have an effect on the final results, however, as our aim was to compare the wood accumulation at different pier geometries, this aspect was considered not relevant.

TABLE 2 Log classes, log dimensions and log mixture

Class	Length (mm)	Diameter (mm)	Log mixture (%)
Small	60	2	80
Medium	90	4	12
Large	150	6	8

The wood density for seasoned and dry beech varies in the range 700–900 kg/m^3. For this reason, before each run, logs were put in a container filled with water for

300 s. This duration was determined based on the maximum duration of each test (in this case 250 s for uncongested transport) to reduce weight fluctuations during the experiments (Welber, Bertoldi, & Tubino, 2013). Additional preliminary tests show that log weight fluctuations during a test are relatively small, being in the range between 2 and 7% for large and small logs, respectively.

Two types of wood transport mechanisms (Braudrick, Grant, Ishikawa, & Ikeda, 1997) were simulated: uncongested (when logs move without contact between them; each piece of wood can move independently of the others) and semi-congested (when the pieces of wood move together as a single mass or entering in contact between them). In the first case, one log each 5 s was introduced at 2.9 m upstream of the flume, along the centreline and oriented parallel to the flow ($\theta = 0$ rad). A total of 50 logs were entered during each run. In the second case, the input frequency was 25 logs together in a cohort every 20 s (the number of tests and tests repetition is reported in Figure 4). The logs were released in the channel centre but randomly oriented with respect to the flow direction. The duration of a single 'uncongested' and 'semi-congested' test was 250 and 100 s, respectively.

2.2.3 | Flow conditions

To obtain different hydraulic conditions the discharge and the downstream sluice gate were regulated. Two different discharges were used for the experiments (Table 3).

These flow conditions are represented by Froude numbers equal to 0.3 and 0.5, which represent conditions for floods in lowland rivers, often characterised by Froude number lower than one (Gippel, O'Neill, Finlayson, & Schnatz, 1996).

Reynolds number was computed using two different regions of the flume, that is, the walls and the flume bed. To quantify the retaining effect of the walls on the main flow the well-known 'Side-Wall Correction Method' of Johnson (1942) with the modification by Vanoni and Brooks (1957) was used. The Reynolds numbers of the bed were of the order of $4/5 \times 10^4$, that are referred to a fully turbulent flow (for bed friction factor of about 6×10^{-2} and Moody type diagram for open channels with impervious rigid boundary [Yen, 2002]).

2.2.4 | Two-dimensional modelling

A two-dimensional numerical model for simulating free surface shallow water flow, *Iber*, has been applied to reproduce the hydrodynamics of the experimental tests (Bladé et al., 2014). To solve the shallow water governing equations, the model applies finite volume method with high-resolution (second order) extension of Roe's scheme. The model interface is based on the preprocess and postprocess software GID. Unstructured calculation meshes reproduced the geometric domain. The model allows assigning different sizes to mesh for different objects depending on the detail level needed. Higher mesh resolution close to the pier was used (0.005 m). The bed roughness, defined in terms of Manning roughness coefficient, was calibrated by comparing the predicted and observed values of flow depth (see Section C in the Supporting Information) and assigned to each element of the mesh and equal to 0.022 s/m$^{1/3}$, based on the comparison between experimental and numerical water depth and flow velocities measured in the flume at the gauging stations indicated in Figure 1.

The two-dimensional numerical simulations were used to define a pier hydraulic-shape coefficient C_{pier}, here introduced for the first time, to characterise the flow field upstream of the pier for the different pier shapes. The obstacle (i.e., pier) produces a loss of energy and modifies the flow upstream and downstream. The pier shape has an effect on the resulted flow, as commonly observed during scour experiments (Richardson & Davis, 2001). Upstream from the pier a 'low flow velocity area' (A_{LFV}) can be observed (Figure 3). A_{LFV} is defined as the flow area conventionally delimited by the streamline where flow velocity is 60% of the flow velocity u_∞ not affected by the presence of the pier and it was calculated from the 2D numerical simulations carried out with different pier shapes. A_{LFV}

TABLE 3 Hydraulic conditions performed in the flume tests

Discharge (m^3/s)	Mean surface flow velocity (m/s)	Water depth (m)	Froude number (−)	Reynolds number (−)	Sluice-gate opening (m)
0.004	0.33	0.04	0.5	$Re_b = 4.21 \times 10^4$ $Re_w = 2.92 \times 10^4$	Weir totally opened
0.006	0.25	0.07	0.3	$Re_b = 5.73 \times 10^4$ $Re_w = 2.04 \times 10^4$	0.02

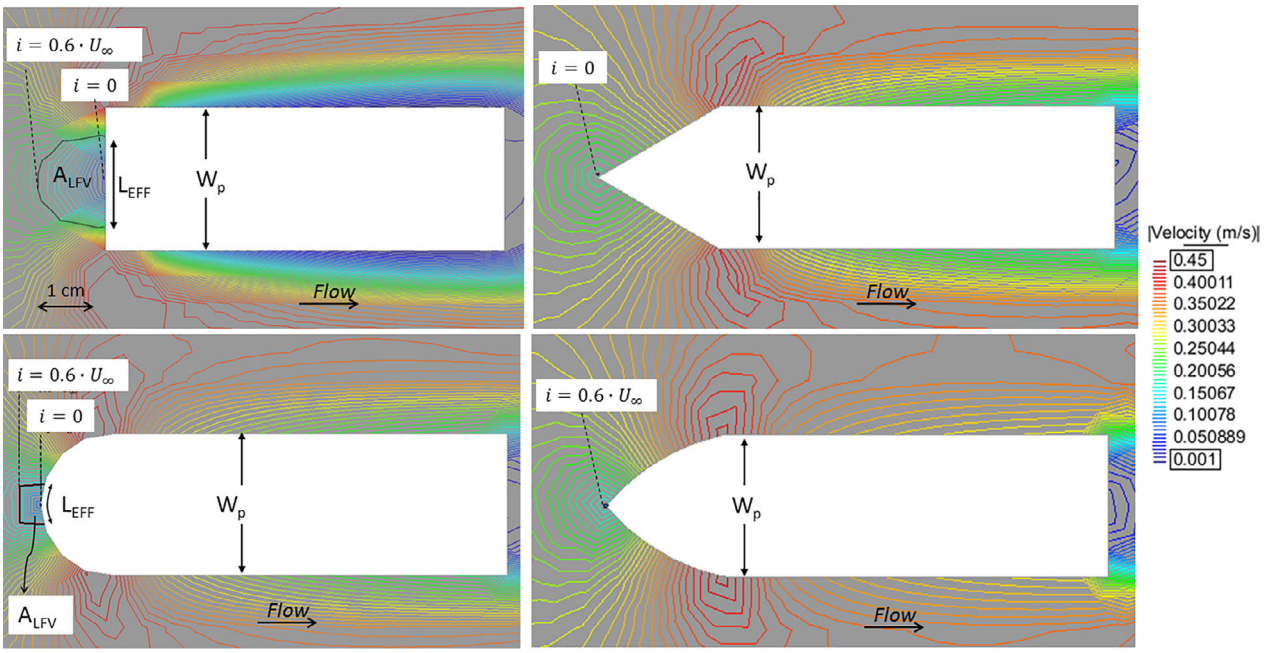

FIGURE 3 Streamlines maps computed by the 2D numerical model in the case of Fr = 0.5

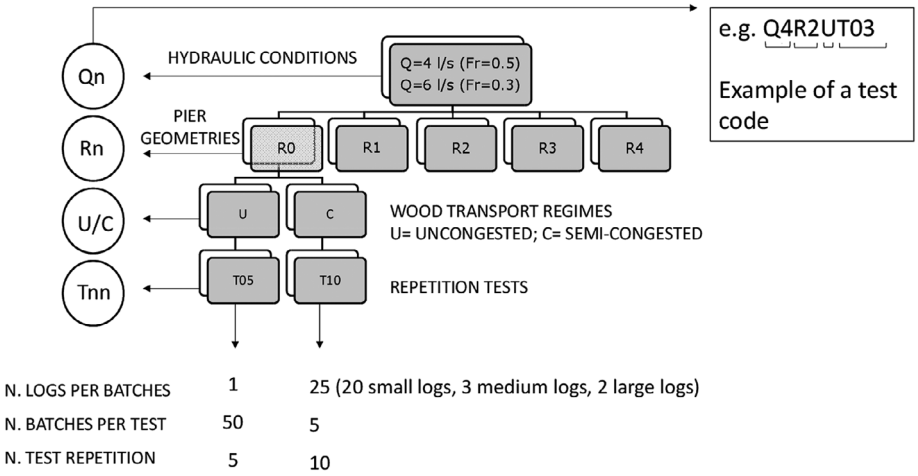

FIGURE 4 Sketch illustrating the experimental tests carried out

appears to be higher around the flat pier shapes, such as the square, rounded, and trapezoidal piers, whereas it becomes negligible around the more pointed pier shapes. Introducing L_{EFF} as the linear projection of A_{LFV} on the pier, the following dimensionless parameter is defined:

$$C_{pier} = \frac{A_{LFV}}{L_{EFF}} \frac{1}{w_p} \quad (1)$$

C_{pier} provides a measure of the impact of the 'low flow velocity area' protruding on the upstream flow field (A_{LFV}/L_{EFF}) relative to the pier width w_p, therefore, it is not only related to the shape of the pier but also to the flow field upstream from the structure. In this regard, it differs from other coefficients provided in the literature as they depend only on the geometry of the pier (e.g., the pier shape factors or parameters proposed by Melville & Coleman, 2000, Richardson & Davis, 2001, Ettema, Constantinescu, & Melville, 2011, or by Ettema, Constantinescu, & Melville, 2017).

We hypothesized that higher values of C_{pier} lead to higher blockage probabilities.

2.2.5 | Model runs and blockage probability

For each pier shape, the two Froude numbers (i.e., 0.3 and 0.5) and the two wood transport mechanisms were

tested. Each test was repeated 5 times for the uncongested transport (1 log for batches and 50 batches per test) and 10 times for the semi-congested transport mechanisms (25 logs per batches and 5 batches per test) (Figure 4), that represents a large enough repetition number for statistically relevant results (Schalko, 2017; Schmocker & Hager, 2010, 2011).

Results were analysed in terms of the blockage probability. The blockage probability (P) refers here as the probability of the wood to accumulate at the bridge pier. Therefore, wood blockage probability is equal to 1 ($P = 1$) when a log is blocked at the pier and $P = 0$ when the log does not stop at the pier (Schmocker & Hager, 2011). This study focused on the interaction between logs and one single central pier, thus the case of pier-to-pier wood accumulation was no investigated.

Following the Buckingham π theorem we can define the dependence of p as:

$$P = f\left(\frac{Q_{\log}}{Q}, \frac{\rho_{\log}}{\rho}, \frac{L_{\log}}{w_{\mathrm{p}}}, \frac{w_{\mathrm{p}}}{L_{\mathrm{p}}}, Fr, Re, C_{\mathrm{pier}}, \alpha_{\mathrm{pier}}, \text{shape of logs}, \theta\right) \quad (2)$$

where Fr and Re are the Froude and Reynolds's respectively, $\frac{w_{\mathrm{p}}}{L_{\mathrm{p}}}, C_{\mathrm{pier}}, \alpha_{\mathrm{pier}}$ define the bridge pier geometry, $L_{\log}$ is the log length, w_{p} and L_{p} are respectively the pier width and length, α_{pier} is the orientation of the pier with respect to the flow direction (see Supporting Information, D), $\frac{Q_{\log}}{Q}, \frac{\rho_{\log}}{\rho}, \frac{L_{\log}}{w_p}$, shape of logs, θ are the wood transport and log characteristics Q is the flow discharge, $Q_{\log}$ is the volumetric log input rate, $\rho_{\log}$ and ρ are the log density and water density, respectively, Finally, the authors define a new coefficient, introduced here for the first time, c_{pier} as the pier hydraulic-shape coefficient that considers the flow velocity field generated upstream of the pier for different pier geometric configurations.

In order to focus the analysis on the influence of pier shape Equation (2) was modified using the following considerations: (a) The logs were reproduced by using wooden cylindrical dowels with no roots and no branches in floating conditions ($\rho_{\log} < \rho$) and randomly oriented with respect to the flow direction, thus the angle θ and $\frac{\rho_{\log}}{\rho}$ and log shapes can be omitted from Equation (2); (b) A single pier was reproduced in the experimental tests, hence the influence of α_{pier} was neglected and L_{p} has no effect on P in the current experiments, and thus the ratio $\frac{w_{\mathrm{p}}}{L_{\mathrm{p}}}$.

Considering the flow as fully turbulent, the Reynolds number was also omitted. After these simplifications, the wood blockage probability at a single central pier can be expressed as:

$$P = f\left(\frac{Q_{\log}}{Q}, \frac{L_{\log}}{w_{\mathrm{p}}}, Fr, C_{\mathrm{pier}}\right) \quad (3)$$

To highlight the effect of different pier shapes on wood accumulation, the experimental results are further explained by introducing the effective blockage probability (P_{e}) and the impact probability (P_{i}) (see Table 4). P_{e} represents the ratio between the number of logs per classes (or for all classes) that are blocked at the pier at the end of each run and the total number of logs introduced in the flume per class (or for all classes). The main difference between P and P_{e} is that in the former case only the actual blockage occurrence is considered, in the latter case also the number of blocked logs is examined. P_{i} is the ratio between the number of logs that impact (i.e., touch) the pier but do not necessarily stop, and the total number of logs introduced in the flume, and it has been introduced as a probability of the potential occurrence of clogging (see Ruiz-Villanueva et al., 2017).

Therefore, two main cases are distinguished for blockage probability definition; (a) if blockage occurs or not (P) and (b) the blockage in relation to the number of entrapped logs (P_{e} and P_{i}). Table 4 summarises the various definitions and the formulas.

3 | RESULTS

3.1 | Blockage probability P versus wood transport mechanism

We observed that P increases for semi-congested wood transport (Figure 5), with values up to 0.9 (i.e., in nine cases out of 10 the logs stopped at the pier), while during uncongested wood transport the highest value of p was just .012. Figure 5 also shows that the flatter pier shapes, such as the square (R0) and the trapezoidal (R4), were the most critical for wood accumulation for both Froude numbers, showing the highest P values. The worst case (i.e., highest blockage probability) was observed for the flat pier shape and Fr = 0.5. The lowest P value ($P = 0$) was obtained for the Ogival pier shape, which was less prone to 'capture' logs during the two wood transport mechanisms and two hydraulic conditions.

During uncongested transport, the higher blocking probability was observed at lower flow velocity condition (i.e., Fr = 0.3) and with the trapezoidal pier shape (R4). For the same hydraulic conditions, logs did not stop at the other four pier shapes. For Fr = 0.5 the logs stopped only at the flatter pier shapes (square R0, rounded R1, and trapezoidal R4).

TABLE 4 Definition and description of the blockage probability functions determined in the flume experiments for both uncongested and semi-congested wood transport

Code	Definition	Formula	Values	Description	Reference
P	Blockage probability	—	0,1 0 = no blockage 1 = yes blockage	Probability of drift to get blocked at the bridge. When drift passes the bridge section the blocking probability is 0 while when it is blocked the probability is 1.	Schmocker & Hager, 2011
P_e	Effective blockage probability	$\frac{\#\text{blocked logs}}{\#\text{input logs}}$	0÷1 0 = no logs *stop* at the pier 1 = all logs *stop* at the pier	The number of logs that *stop* at the pier at the end of the test. It represents the 'effective' blockage probability.	This study
P_i	Impact probability	$\frac{\#\text{logs touch}}{\#\text{input logs}}$	0÷1 0 = no logs impact the pier 1 = all logs impact the pier	The number of logs that *impact* or *touch* the pier after each impulse of logs. It represents the 'potential' blockage probability.	This study after Ruiz-Villanueva, Wyżga, Mikuś, Hajdukiewicz, & Stoffel, 2017

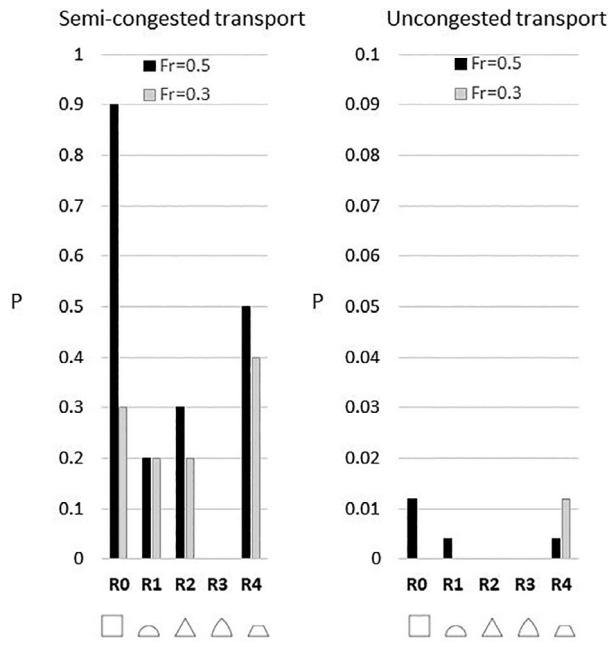

FIGURE 5 Blockage probability P for congested and semi-congested wood transport, different pier shapes

3.2 | Blockage probability *P* versus wood size

The blockage probability (P) plotted versus the relative log size (L_{log}/w_p) (Figure 6), shows that, even if large logs ($L_{log}/w_p = 6$) are less frequent (8% of the total logs versus the 80% of the small logs), the probability to block at the pier was relatively high (e.g., the flat pier shape and Fr = 0.5) and frequent (e.g., for Fr = 0.3 large logs blocked in correspondence of four pier shapes on five). For higher flow velocity, that is, Fr = 0.5, all log sizes stopped at the flat pier shape (R0), while at the rounded pier shape (R1), only the smaller logs blocked. Larger logs were more easily trapped at the flat (R0) and triangular (R2) piers. No logs stopped at the Ogival pier (R3) for both hydraulic conditions.

In case of lower flow velocity (Fr = 0.3) the highest probability for small and large logs was observed for the trapezoidal pier shape (R4), as shown in Figure 6. All log sizes stopped only at the triangular pier (R2) while the large and small logs stopped at all pier shapes except for the Ogival (R3). For logs with the same length, for example, the small logs, the blockage probability is higher when the flow velocity is higher (Fr = 0.5). This is not the case for medium and large logs for which, in most cases, the blockage probability was higher at lower flow velocity (Fr = 0.3) than at higher flow velocity (Fr = 0.5).

3.3 | Blockage probability *P* versus flow field

The flow velocity and thus the Froude number affected the log motion and consequently the blockage probability. Figures 5 and 6 show that in most analysed cases, the blockage probability is higher at Fr = 0.5 (Q = 0.004 m^3/s) than at Fr = 0.3 (Q = 0.006 m^3/s) for the experimental conditions.

Figure 7 shows that the flow surface velocity distribution measured at different cross-sections along the flume influenced the logs trajectory observed in the flume.

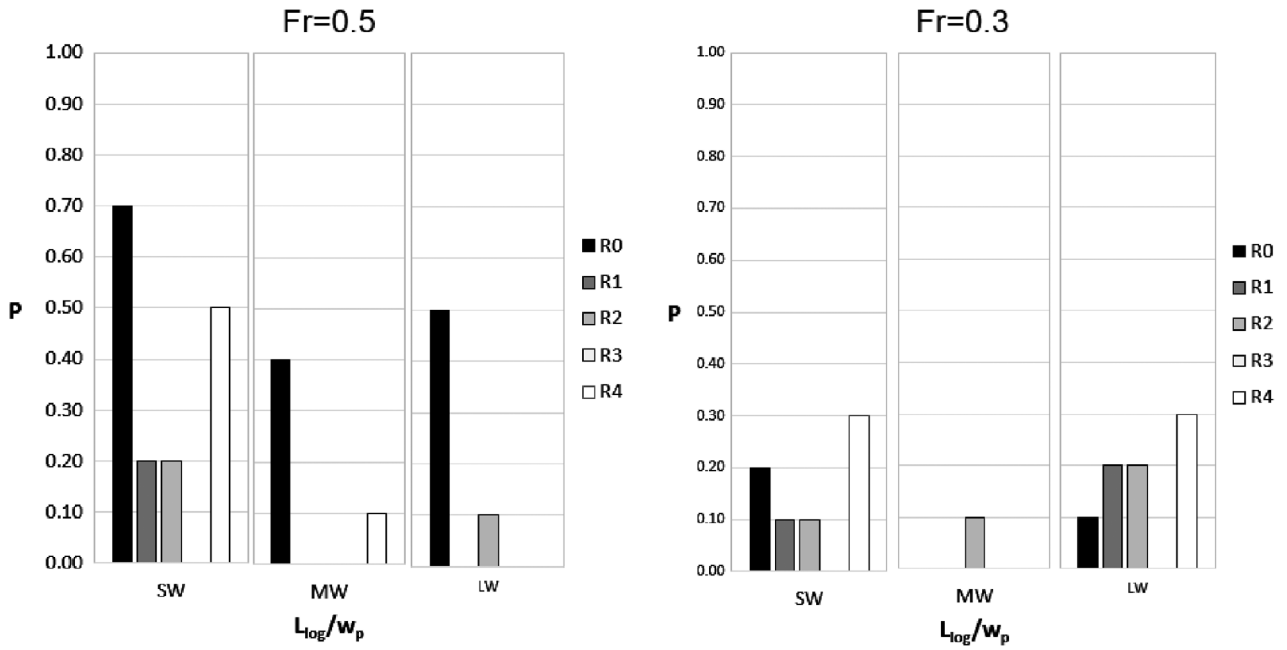

FIGURE 6 Blockage probability P versus L_{log}/w_p for Fr = 0.5 and Fr = 0.3. LW, large wood; MW, medium wood; SW, small wood

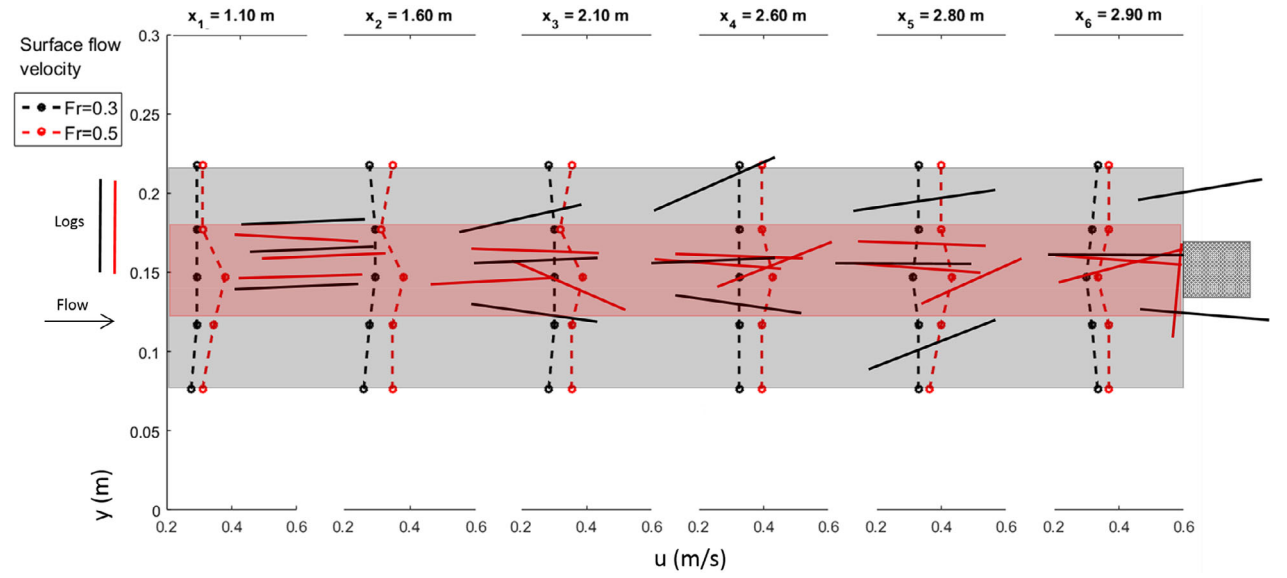

FIGURE 7 Scheme of the log movement observed in flume experiment (top view). The grey and red zones are the areas occupied by the logs (black and red lines) while transported at Fr = 0.3 and Fr = 0.5, respectively. The dotted dashed lines represent the flow velocity distribution measured in flume

The measured flow velocity cross-sectional distribution (red and black dots in Figure 7) shows that for Fr = 0.3 (black dots) the velocity distribution is rather uniform through the section. Contrasting, for Fr = 0.5 (red dots) the velocity is higher in the middle of the flume width. Logs followed this higher velocity line, moving along the centreline, and therefore, they were more prone to interact with the pier which was located in their trajectory (see red segments in Figure 7).

3.4 | Blockage probability *P* versus pier hydraulic-shape coefficient C_{pier}

The low flow velocity area A_{LFV} and C_{pier} were estimated from two-dimensional numerical simulations in the case of Fr = 0.5 that gave a higher correlation coefficient of predicted-observed flow depth and depth-averaged flow velocity (see Section C in the Supporting Information). The pier hydraulic-shape coefficients for each pier shape

TABLE 5 Values of pier hydraulic-shape coefficient for different pier shapes and Fr = 0.5

Code	Geometry	Figure	A_{LFV} (cm^2)	L_{EFF} (cm)	C_{pier}
R0	Square-nose		1.235	1.524	0.324
R1	Round-nose		0.065	0.35	0.075
R2	Triangular-nose (60°)		0.0001	0.01	0.005
R3	Ogival-nose		0.0002	0.04	0.002
R4	Trapezoidal-nose		0.073	0.31	0.095

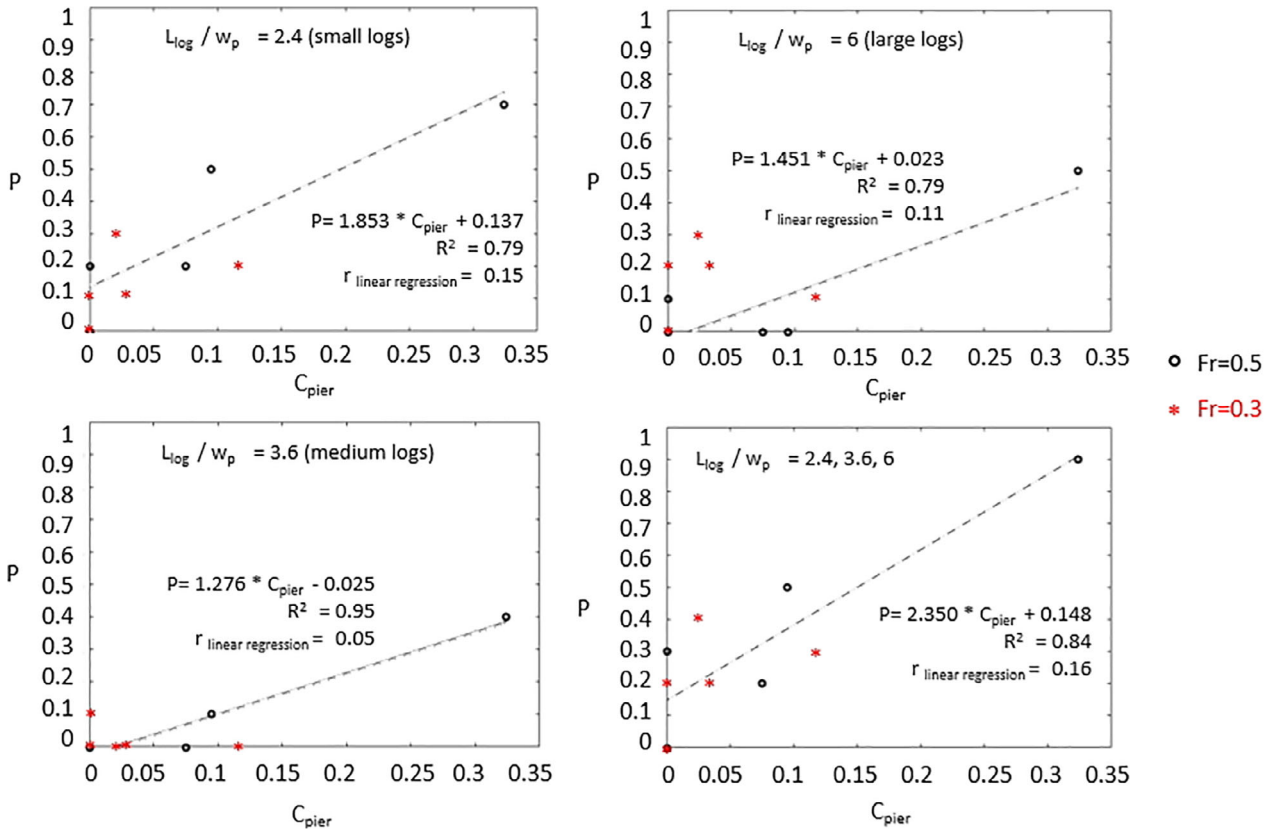

FIGURE 8 Blockage probability P versus pier hydraulic-shape coefficient C_{pier} for each class of log size and for all log size classes, and Fr = 0.5. $r_{linear\ regression}$ is the cumulative deviation of data from the regression line (*SD* about the regression)

are listed in Table 5. In two cases $C_{pier} = 0$, for the triangular and Ogival pier shapes, both characterised by a more pointed pier shape. The highest value was obtained for the rectangular pier, meaning that the flatter the pier cutwater the higher the low flow velocity area upstream of the pier (A_{LFV}) and thus C_{pier} (see Equation 1). The correlation between blockage probability and pier hydraulic-shape coefficient for different ratio (L_{log}/w_p) and for all log size classes and Fr = 0.5 is presented in Figure 8.

In all cases the blockage probability P increases with increasing C_{pier}. The relation (see dashed-line fits in Figure 8) between the pier shape and the blockage probability shows that the geometry of the pier has an important effect on the flow field upstream of the pier and thus on the log motion and its blockage.

3.5 | Effective wood blockage probability (P_e) and impact wood probability (P_i)

According to our results, the lowest blockage probability was observed for the Ogival pier (R3), both in terms of effective blockage probability and impact probability (Figure 9).

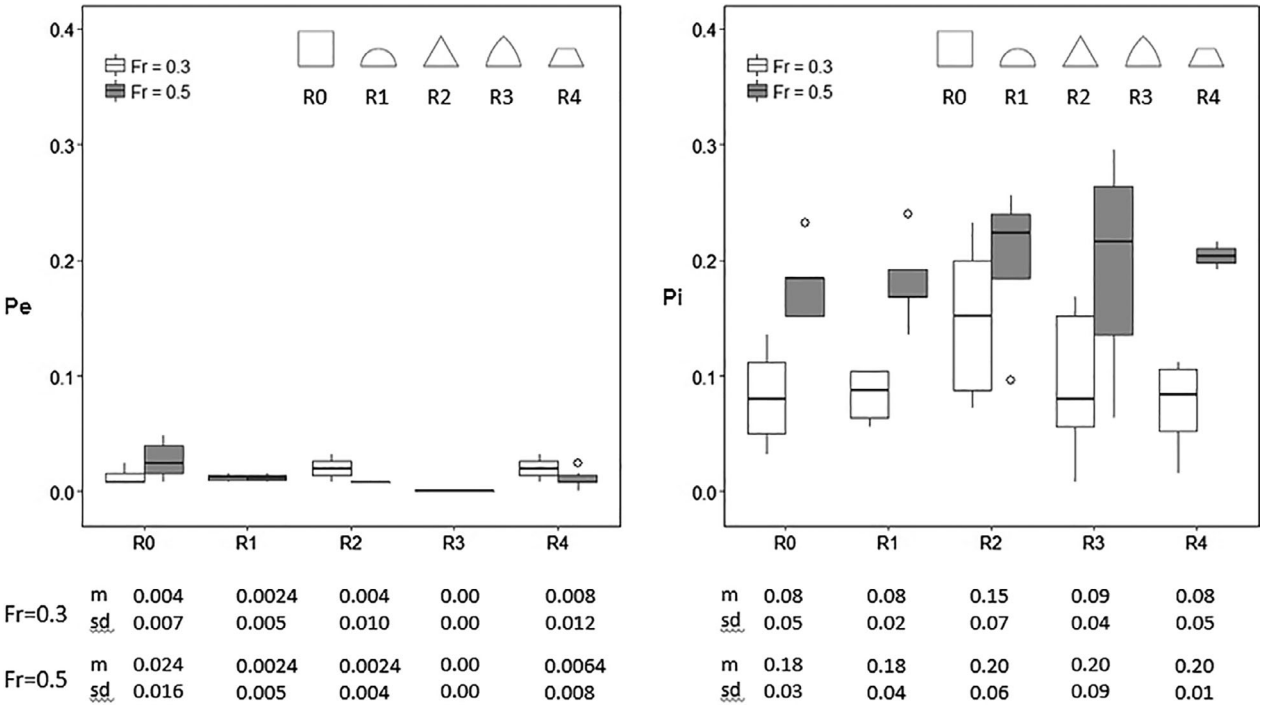

FIGURE 9 Effective blockage probability P_e (left) and impact probability P_i (right) for different pier shapes and Froude numbers in congested transport mechanism (m = median; SD = standard deviation)

However, high values of impact probability (P_i) do not always correspond with high values of effective blockage probability (P_e). For Fr = 0.5 and Fr = 0.3 the highest mean value of p_i was obtained for the triangular pier shape (R2) while the highest mean value of P_e for Fr = 0.5 was obtained for the flat pier shape (R0). The impact probability for all pier shapes (P_i) (Figure 9, on right) ranges between 0 and 30% while the effective blockage probability (P_e) (Figure 9, on left) is lower than 10%. Therefore, the range of P_e/P_i is between 0 and 30%. Not all the logs that touch the pier stop at it. In this way, the pier shape may favour or not the log stopping: this is the case of the Ogival pier for which the impact probability ranges between 18 and 22%, while the effective blockage probability is zero. The impact probability is higher at Fr = 0.5 than Fr = 0.3, likely due to the tendency of logs to move mainly in the centreline in the first case, as explained previously and schematized in Figure 7, and related to the flow velocity distribution measured in flume along the cross-sections upstream of the pier.

4 | DISCUSSION

This work aimed at investigating the factors controlling wood accumulation at a single pier, studying a combination of different pier shapes (with a focus on pier shapes typical of historical cities), different wood transport mechanisms, and hydraulic conditions (i.e., different Froude numbers but always in subcritical conditions) and defining a blockage function. In the present study, physical modelling was carried out with the aim of simulating wood blockage at bridge piers, and analyse the effect of the pier shape on this blockage, rather than reproducing a specific field case (as in Bertoldi, Welber, Mao, Zanella, & Comiti, 2014; Parola et al., 2000; Welber et al., 2013). It is worth pointing out that the dimensions of channels and logs in the present model were inspired by field observations in the Arno River, but not precisely scaled from a specific prototype. Therefore, the resulted blockage probabilities calculated are representative of straight, large rivers and must be analysed in a relative and comparative way (i.e., comparing the blockage probability obtained for the different pier shapes).

4.1 | Effects of bridge pier on the streamline pattern

We carried out experiments under two different flow conditions, Fr = 0.3 and Fr = 0.5, constrained by the flume facility used, but which are typical conditions for large lowland rivers that can occur at floods. We observed differences in the blockage probability under these two flow scenarios, however, different conditions may lead to different blockage probabilities. The aim of our study was to

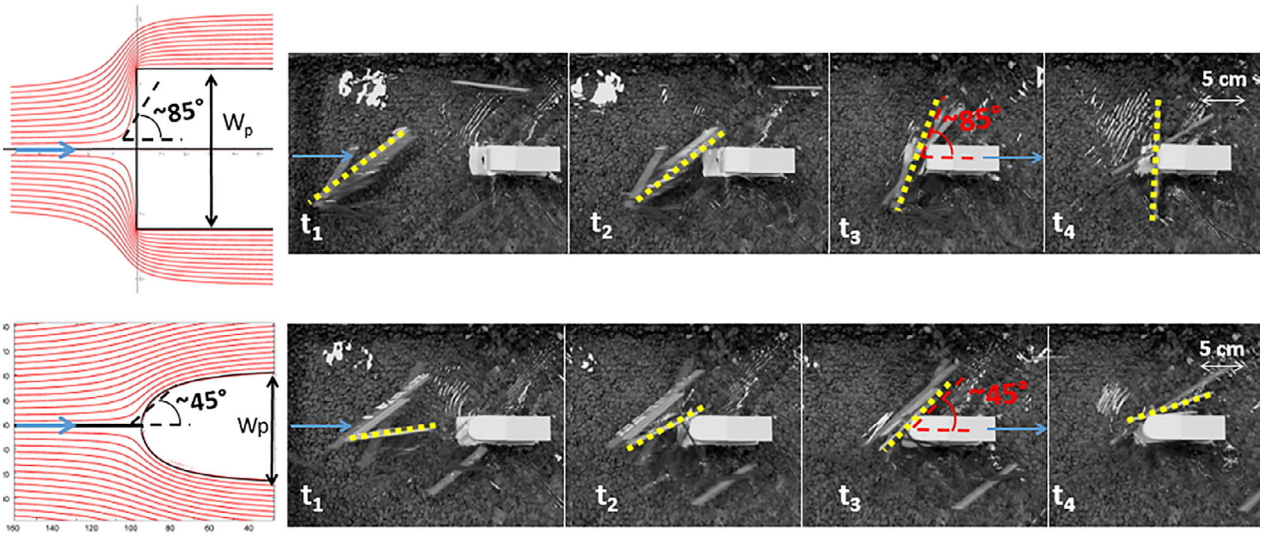

FIGURE 10 (a) Experimental observation on orientation and travelled path logs approaching the flat pier (upper panel) and the rounded pier (lower panel) at four different time intervals (flow direction from left to right). (b) Streamlines at a flat pier shape (upper panel) and semi-circular pier shape (lower panel). Flow from right to left

see the effect of different pier geometries under two different flow conditions, and not to compute wood blockage for a large range of Froude number, additional tests would be required for the latter (Box, Hunter, & Hunter, 1978).

Potential flow theory can provide a preliminary interpretation to explain the experimental observation of the log movements in the flume. The 2D streamlines around the pier are analytically derived by assuming the flow has a negligible vertical component of vorticity on the water surface. Under this assumption, the stream function upstream of the pier is obtained in two different representative cases: the rounded pier and the square pier. The rounded pier is modelled as a Rankine Half-Body while the squared pier as a Schwarz–Christoffel transformation applied to a half plane (Kundu & Cohen, 2008). The streamlines in Figure 10, b at Fr = 0.5, show that the angle between the main flow direction and the tangent to the curve of the streamline is about 85° for the flat pier shape and about 45° for the rounded pier. In the former case, the log undergoes a greater rotation with respect to the main flow direction and then it flows downstream; in the latter case, the rotation angle is lower and the log easily follows the flow.

Most of the experimental observations confirmed the simplified theoretical analysis of the streamlines, as illustrated in Figure 10a, that shows the time-lapse sequence of congested transport of logs at the flat pier shape (upper panel) and at the rounded pier (lower panel). The yellow dashed line shows the travelled path and orientation of one single log s close to the pier frontal side. At the time step t_3 the log touches the pier following the curvature of the streamlines as represented in Figure 10b. At the flat pier shape (upper panel) the log centre moves along the stagnation point and it gets blocked at the pier; at the rounded pier (lower panel), even if the log centre moves close to the stagnation point, the lower curvature causes the log sliding. This confirms also the higher blockage probability for Fr = 0.5 (see Figure 5 on left) at the flat pier shape ($P = 0.9$) than at the rounded pier ($P = 0.2$). The potential flow theory (see Figure 10) showed the streamlines curvature generated by different pier shapes and what may happen if the log follows the stagnation streamline.

The blockage probability is higher for the flat pier shape where the streamline curvature upstream of the pier is higher. However, this depends on the orientation of the log with respect to the flow, the alignment of the log with respect to the pier (if the log follows the stagnation streamline or the streamlines close to it), the log length, and the local changes in depth and velocity fields. The explanation for the different log motion depending on the flow hydraulics may be attributed also to the secondary flow generation. The vortex of secondary currents may be stronger towards the centreline in one case (Fr = 0.5) than the other (Fr = 0.3) (Albayrak & Lemmin, 2011). The experimental observation on the orientation and track logs approaching the pier confirms the results of Adachi and Daido (1957). These authors did not analyse the effect of the pier shape on the wood-pier interaction, but just the cases for wood to pass after touching the pier (here defined as impact probability). Adachi and Daido (1957) defined the percentage of logs to be washed away after touching the pier depending on the way in

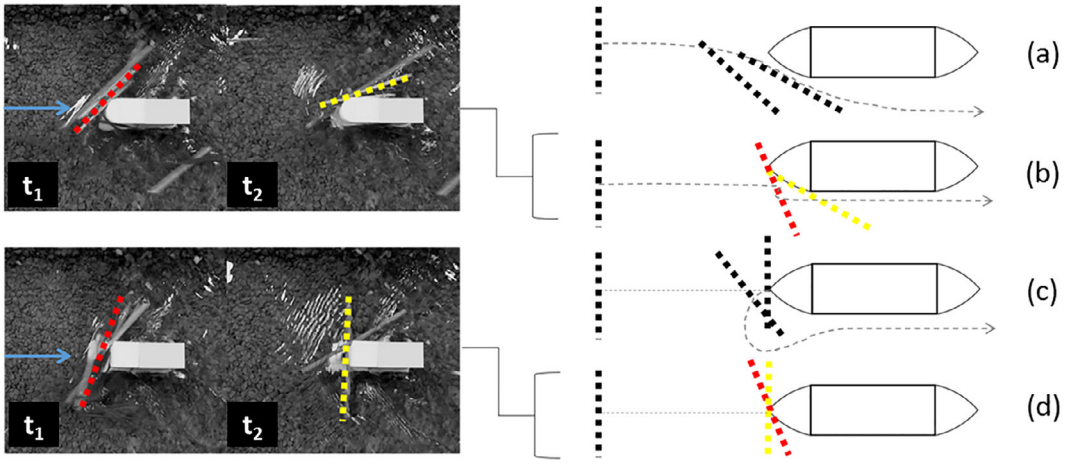

FIGURE 11 Possible configurations for logs to be washed away, on the right (adapted from Adachi & Daido, 1957) compared with the experimental observation presented in the current research, on the left. The coloured lines indicate the configurations proposed by Adachi and Daido (1957) observed in flume experiments

which the log approaches the pier. The tests were performed in subcritical conditions (Fr = 0.08/0.4). The Figure 11 (right) represent four main cases: (a) when the log passes without touching the pier; (b) the log touches the pier and slides down; (c) the log bumps into the pier and bounces backward and then it flows away; and (d) the log bumps into the pier and the pressure of the running water on the left and right of the log is balanced, so the log stops at the pier. The cases (a), (b), and (c) represent what the authors here defined as impact probability (P_i) while the case (d) is the effective blockage probability (P_e).

Although Figure 11 illustrates the case of logs introduced in the flume perpendicular to the flow, the authors (Adachi & Daido, 1957) affirm to obtain quite similar results for logs introduced parallel to the flow direction. The highest percentage of logs blocked at the pier was obtained with Fr = 0.4 and in the case (d). In the current research, the cases (c) and (d) were observed more often at Fr = 0.5, when the logs moved mainly in the centreline and the blockage probability was greater, while the cases (a) and (b) were more frequent at Fr = 0.3, when the logs moved both in the centreline and towards the walls. Figure 11 shows the comparison between the experimental observations by Adachi and Daido (1957) and the present experimental observations for cases (b) and (d) revealing similar results.

In our experiments, we entered the logs 2.9 m upstream from the pier, and this has an influence on the results. Logs, independently from the initial orientation (in general parallel to the flow direction) adjusted their trajectory approaching the pier aligned with the flow, and in general, they behaved as tracers. Changing this set up, adding the logs to the flume non-parallel to the flow and closer to the pier would lead to different results, such as higher blockage probability for decreasing approach flow velocity (Schalko, 2017). This is explained because under those conditions, logs may not behave like tracers, but they are affected by an acceleration due to the difference between the flow velocity and their actual velocity. Therefore, the experiment set up is very relevant and should be designed carefully to fulfil the objectives of the study. In our case, the goal was to test relative differences between the different pier shapes and not to compute absolute blockage probabilities.

4.2 | Effects of logs shape on blockage probability

Finally, blockage probability may be influenced by the shape of the logs. In our experiments, cylinders with no roots and no branches were used.

Although this type of logs has been widely used in flume experiments (Bertoldi et al., 2014, 2015; Bocchiola, Rulli, & Rosso, 2006; Braudrick et al., 1997; Braudrick & Grant, 2001; Welber et al., 2013), the presence of branches and roots may increase the blockage probability as logs with branches (or roots) may more easily interact with each other and with the pier (Lyn et al., 2003; Schmocker et al., 2013). Thus, the blockage probability P here determined represents the minimum predicted probability.

As our aim was to analyse the effect of different pier shapes on the blockage probability in a comparative way rather than calculating its absolute value, we consider this simplification as acceptable.

5 | CONCLUSIONS

In the present work, wood accumulation at a single bridge pier with different shapes was investigated experimentally and through numerical modelling. The aim was to test the influence of the pier geometry on the wood blockage probability. To do that, we designed the experiments using two wood transport mechanisms, different log size classes, two flow conditions, and five pier shapes. This research showed that:

- the wood blockage probability P at a single pier was significantly influenced by the wood transport mechanisms, with higher P under semi-congested wood transport;
- P was higher under Fr = 0.5 rather than Fr = 0.3 for the experimental conditions; this was due to different flow field configurations upstream of the pier;
- the flow field upstream of the pier was greatly influenced by the pier geometry, and thus the latter affected the blockage probability P. Wood blockage probability at the flat pier shape resulted three times greater than the triangular shaped pier (for semi-congested transport mechanisms and Fr = 0.5); in case of an Ogival pier, zero blockage probability was found for both Froude number investigated;
- the relationship between P and log length over pier width (L_{log}/w_p) revealed that largest logs, even if low in number, stopped at the pier with a relatively high frequency.

The results from the current research may provide a support to design bridge or countermeasures aimed at minimising wood accumulation at pier shapes typical of historical cities. In this regard, field data on wood transport (especially during high-magnitude flood events) and accumulation at bridges, are needed. The lack or insufficient field data constitute one of the main problems for researchers. The monitoring activity and the implementation of multiple processes and factors such as sediment transport, the complex nature of log shapes (incl. Roots and branches), the number of piers, as well as different river morphologies. The combination of numerical modelling, together with experiments is a powerful approach for prevention strategies.

ACKNOWLEDGEMENTS

The authors would like to thank the BSc students for their support in the experimental activity and the Mauro Gioli and Muzio Mascherini for their laboratory assistance. The authors thank four anonymous reviewers for their comments which help to significantly improve the early version of this manuscript.

NOTATION

C_{pier}	pier hydraulic-shape coefficient
D_{log}	log diameter
Fr	Froude number
h	Water depth
L_{log}	log length
L_p	pier length
P	blockage probability
P_e	effective blockage probability
P_i	impact probability
Q	flow discharge
Q_{log}	volumetric log input rate
Re	Reynolds number
U_∞	undisturbed free stream velocity
w	channel width
w_p	pier width
α_{pier}	orientation of the pier with respect to the flow direction
θ	inclination of the log relative to the flow direction
ρ	water density
ρ_{log}	density of wood

DATA AVAILABILITY STATEMENT

The data that support the findings of this study are openly available in the repository zenodo.org and can be downloaded at http://doi.org/10.5281/zenodo.3541603.

ORCID

Luca Solari https://orcid.org/0000-0001-9227-4305

REFERENCES

Adachi, S. & Daido, A. (1957). Experimental study on washed timbers (No. 1, pp. 41–49). In Annual Report of Disaster Prevention Research Institute, Kyoto University.

Albayrak, I., & Lemmin, U. (2011). Secondary currents and corresponding surface velocity patterns in a turbulent open-channel flow over a rough bed. *Journal of Hydraulic Engineering*, *137*(11), 1318–1334.

Allen, J. B., & Smith, D. L. (2012). Characterizing the impact of geometric simplification on large woody debris using CFD. *International Journal of Hydrogen Energy*, *1*, 1–14. https://doi.org/10.5923/j.ijhe.20120102.01

Badoux, A., Böckli, M., Rickenmann, D., Rickli, C., Ruiz-Villanueva, V., Zurbrügg, S., & Stoffel, M. (2015). Large wood transported during the exceptional flood event of July 24, 2014 in the Emme catchment (Switzerland). In Proceedings of the third International Conference Wood in World Rivers 2015 (pp. 109–111), Padova, Italy.

Benda, L. E., & Sias, J. C. (2003). A quantitative framework for evaluating the mass balance of in-stream organic debris. *Forest Ecology and Management*, *172*(1), 1–16. https://doi.org/10.1016/S0378-1127(01)00576-X

Benke, A. C., & Wallace, B. J. (2003). Influence of wood on invertebrate communities in streams and rivers. In S. V. Gregory, K. L. Boyer, & A. M. Gurnell (Eds.), *The ecology and management of wood in world rivers* (pp. 149–177). American Fisheries Society, Symposium 37, Bethesda, MD.

Bertoldi, W., Welber, M., Gurnell, A., Mao, L., Comiti, F., Tal, M. (2015). Physical modelling ofthe combined effect of vegetation and wood on river morphology. *Geomorphology 246*, 178–187. https://doi.org/10.1016/j.geomorph.2015.05.038.

Bertoldi, W., Welber, M., Mao, L., Zanella, S., & Comiti, F. (2014). A flume experiment on wood storage and remobilization in braided river systems. *Earth Surface Processes and Landforms*, *39*, 804–813. https://doi.org/10.1002/esp.3537

Bladé, E., Cea, L., Corestein, G., Escolano, E., Puertas, J., Vázquez-Cendón, E., Dolz, J., & Coll, A. (2014). Iber: herramienta de simulación numérica del flujo en ríos. *Revista Internacional de Métodos Numéricos Para Cálculo y Diseño en Ingeniería*, *30* (1), 1–10.

Bocchiola, D., Rulli, M. C., & Rosso, R. (2006). Flume experiments on wood entrainment in rivers. *Advances in Water Resources*, *29*(8), 1182–1195. doi.org/10.1016/j.advwatres.2005.09.006

Bocchiola, D., Rulli, M. C., & Rosso, R. (2008). A flume experiment on the formation of wood jams in Rivers. *Water Resources Research*, *44*(2), 1–17. https://doi.org/10.1029/2006WR005846

Box G.E.P., Hunter W.J., Hunter J, 1978. *Statistics for experimenters, an introduction to design, data analysis and model building*. (ISBN 0-471-09315-7). New York: Wiley.

Braudrick, C. A., Grant, G. E., Ishikawa, Y., & Ikeda, H. (1997). Dynamics of wood transport in streams, a flume experiment. *Earth Surface Processes and Landforms*, *22*, 669–683. https://doi.org/10.1002/(SICI)1096-9837(199707)22:7<669::AID-ESP740>3.0.CO;2-L

Braudrick, C. A., & Grant, G. E. (2001). Transport and deposition of large woody debris in streams, a flume experiment. *Geomorphology*, *41*(4), 263–283. https://doi.org/10.1016/S0169-555X(01)00058-7

Comiti, F. (2012). How natural are alpine mountain rivers? Evidence from the Italian Alps. *Earth Surface Processes and Landforms*, *37*, 693–707.

Comiti, F., Lucía, A., & Rickenmann, D. (2016). Large wood recruitment and transport during large floods: A review. *Geomorphology*, 269, 23–39. https://doi.org/10.1016/j.geomorph.2016.06.016.

De Cicco, P. N., Paris, E., Ruiz-Villanueva, V., Solari, L., & Stoffel, M. (2018). In-channel wood-related hazards at bridges: A review. *River Research and Applications*, *34*, 1–12. https://doi.org/10.1002/rra.3300

De Cicco, P. N., Paris, E., & Solari, L. (2016). Wood accumulation at bridges: Laboratory experiments on the effects of pier shape. In *Proceeding of the Eight International Conference on Fluvial Hydraulics*. St. Louis, MO, 12–15 July, 2016.

Diehl, T. H. (1997). *Potential drift accumulation at bridges* (Report No. FHWA-RD-97028). Washington, DC: U.S. Department of Transportation, Federal Highway Administration.

Ettema, R., Constantinescu, G., & Melville, B. W. (2017). Flow-field complexity and design estimation of pier-scour depth: Sixty years since Laursen and Toch. *Journal of Hydraulic Engineering*, *143*(9), 03117006.

Ettema, R., Constantinescu, G., & Melville, B. W. (2011). *Evaluation of bridge scour research: Pier scour processes and predictions* (NCHRP Web-Only Report No. 175). Washington, DC: National Cooperative Highway Program.

Gippel, C. J., O'Neill, I. C., Finlayson, B. L., & Schnatz, I. (1996). Hydraulic guidelines for the re-introduction and management of large woody debris in lowland rivers. *Regulated Rivers: Research Management*, *12*, 223–236. https://doi.org/10.1002/(SICI)1099-1646(199603)12:2/3<223::AID-RRR391>3.0.CO;2-#

Gschnitzer, T., Gems, B., Aufleger, M., Mazzorana, B., & Comiti, F. (2013). Physical scale model test on bridge clogging. *Proceedings of the 35th IAHR World Congress*. Beijing, China: Tsinghua University Press, 2013, ISBN 978–7–89414-588-8, elektronisch.

Gschnitzer, T., Gems, B., Mazzorana, B., & Aufleger, M. (2017). Towards a robust assessment of bridge clogging processes in flood risk management. *Geomorphology*, *279*, 128–140. https://doi.org/10.1016/j.geomorph.2016.11.002

Gurnell, A. (2013). Wood in fluvial systems (Chapter 236–9.11). *Treatise on Geomorphology*, *9*, 163–188.

Harmon, M. E., Franklin, J. F., & Swanson, F. J. (1986). Ecology of coarse woody debris in temperate ecosystems. *Advances in Ecological Research*, *15*, 133–302. https://doi.org/10.1016/S0065-2504(08)60121-X

Iroumé, A., Ruiz-Villanueva, V., & Picco, L. (2017). Breakdown of instream wood in low order forested streams of the southern Chilean mountain ranges. *Forest Ecology and Management*, *401*, 17–32.

Johnson, J. W. (1942). The importance of side-wall friction in bed-load investigations. *Civil Engineering*, *12*(6), 329–331.

Kail, J., Hering, D., Muhar, S., Gerhard, M., & Preis, S. (2007). The use of large wood in stream restoration, experiences from 50 projects in Germany and Austria. *Journal of Applied Ecology*, *44*(6), 1145–1155. https://doi.org/10.1111/j.1365-2664.2007.01401.x

Kattell, J., & Eriksson, M. (1998). *Bridge scour evaluation: Screening, analysis, and countermeasures* (Pub. Report No. 9877). Washington, DC: USDA Forest Service.

Kramer, N., & Wohl, E. (2014). Estimating fluvial wood discharge using time-lapse photography with varying sampling intervals. *Earth Surface Processes and Landforms*, *39*(6), 844–852. http://doi.org/10.1002/esp.3540

Kundu, P. K., & Cohen, I. M. (2008). *Fluid mechanics* (4th ed.). San Diego, USA: Academic.

Lagasse, P. F., Clopper, P. E., Zevenbergen, L. W., Spitz, W. J., & Girard, L. G. (2010). *Effects of debris on bridge pier scour* (NCHRP Report No. 653). Washington, DC: Transportation Research Record. Retrieved from http://onlinepubs.trb.org/onlinepubs/nchrp/nchrp_rpt_653.pdf.

Le Lay, Y.-F., Piégay, H., & Moulin, B. (2013). Wood entrance, deposition, transfer and effects on fluvial forms and processes: problem statements and challenging issues. In J. Shroder (Editor in Chief), D. R. Butler, & C. R. Hupp (Eds.), *Treatise on Geomorphology* (Vol. 12, pp. 20–36). *Ecogeomorphology*. San Diego, CA: Academic Press.

Lyn, D. A., Cooper, T., Yi, Y. K., Sinha, R. N., & Rao, A. R. (2003). *Debris accumulation at bridge crossings, laboratory and field studies*. TRB Subject Code: 25–1 (Publication No. FHWA/IN/JTRP-2003/10, SPR-2478).

Lyn, D., Cooper, T., Condon, D., & Gan, L. (2007). *Factors in debris accumulation at bridge piers, Washington*. Federal

Highway Administration Research and Development, Turner-Fairbank Highway Research Center: U.S. Department of Transportation.

Manners, R. B., Doyle, M. W., & Small, M. J. (2007). Structure and hydraulics of natural woody debris jams. *Water Resources Research*, *43*(6), 17. https://doi.org/10.1029/2006WR004910

Melville, B., & Dongol, D. (1992). Bridge pier scour with debris accumulation. *Journal of Hydraulic Engineering*, *118*, 1306–1310. https://doi.org/10.1061/(ASCE)0733-9429(1992)118:9(1306)

Melville, B. W., & Coleman, S. E. (2000). *Bridge scour*. Highlands Ranch, CO: Water Resource Publications, LLC.

Okamoto, T., Takebayashi, H., Sanjou, M., Suzuki, R., & Toda, K. (2019). Log jam formation at bridges and the effect on floodplain flow: A flume experiment. *Journal of Flood Risk Management*, *13*(S1), e12562. https://doi.org/10.1111/jfr3.12562

Pagliara, S., & Carnacina, I. (2011). Influence of large woody debris on sediment scour at bridge piers. *International Journal of Sediment Research*, *26*(2), 121–136. https://doi.org/10.1016/S1001-6279(11)60081-4

Parola, A. C., Apelt, C. J., & Jempson, M. A. (2000). *Debris forces on highway bridges* (NCHRP Report No. 445). Washington, DC: Transportation Research Board.

Richardson, E. V., & Davis, S. R. (2001). *Evaluating scour at bridges* (4th ed.). Washington, DC: Federal Highway Administration, U.S. Dept. of Transportation.

Ruiz-Villanueva, V., Bladé Castellet, E., Sánchez-Juny, M., Marti-Cardona, B., Díez-Herrero, A., & Bodoque, J. M. (2014). Two-dimensional numerical modeling of wood transport. *Journal of Hydroinformatics*, *16*(5), 1077–1449. https://doi.org/10.1002/esp.3456

Ruiz-Villanueva, V., Piégay, H., Gurnell, A. A., Marston, R. A., & Stoffel, M. (2016). Recent advances quantifying the large wood dynamics in river basins: New methods and remaining challenges. *Reviews of Geophysics*, *1–42*, 611–652. https://doi.org/10.1002/2015RG000514

Ruiz-Villanueva, V., Wyżga, B., Mikuś, P., Hajdukiewicz, M., & Stoffel, M. (2017). Large wood clogging during floods in a gravel-bed river: The Długopole bridge in the Czarny Dunajec River Poland. *Earth Surface Processes and Landforms*, *42*, 516–530. https://doi.org/10.1002/esp.4091

Schalko, I., Schmocker, L., Weitbrecht, V., & Boes, R. M. (2016). Modeling the effect of organic fine material in a driftwood accumulation on backwater rise. In Constantinescu, Garcia & Hanes (Eds.), *Proceedings River Flow 2016*, St. Louis, MO, ISBN 978-1-315-64447-9: 2326-2332.

Schalko, I. (2017). Large wood accumulation probability at a single bridge pier. In Proceedings of 37th IAHR World Congress, August 13–18, 2017, Kuala Lumpur, Malaysia 7710, 1704–1713.

Schmocker, L., & W. H. Hager (2010). Drift accumulation at river bridges. River flow 2010 - Dittrich, Koll, Aberle & Geisenhainer (Eds.), *Proceeding of 8th River Flow Congress 2010*, Braunschweig, Germany, pp 713–720.

Schmocker, L., & Hager, W. H. (2011). Probability of drift blockage at bridge decks. *Journal of Hydraulic Engineering*, *137*(4), 470–479. https://doi.org/10.1061/(ASCE)HY.1943-7900.0000319

Schmocker, L., and W. H. Hager. (2013). "Scale modelling of wooden debris accumulation at a debris rack." *J. Hydraul. Eng.* *139* (8): 827–836. https://doi.org/10.1061/(ASCE)HY.1943-7900.0000714

Solari, L., Van Oorschot, M., Hendriks, D., Rinaldi, M., & Vargas-Luna, A. (2015). Advances on modelling riparian vegetation-hydromorphology interactions. *River Research and Applications*, *32*, 164–178. https://doi.org/10.1002/rra.2910

Steeb, N., Rickenmann, D., Badoux, A., Rickli, C., & Waldner, P. (2017). Large wood recruitment processes and transported volumes in Swiss mountain streams during the extreme flood of august 2005. *Geomorphology*, *279*, 112–127. https://doi.org/10.1016/j.geomorph.2016.10.011

Vanoni, V. A., & Brooks, N. H. (1957). *Laboratory studies of the roughness and suspended load of alluvial streams* (Report No. E-68). Pasadena, CA: Sedimentation Laboratory, California Institute of Technology.

Welber, M., Bertoldi, W., & Tubino, M. (2013). Wood dispersal in braided streams: Results from physical modeling. *Water Resources Research*, *49*, 7388–7400. https://doi.org/10.1002/2013WR014046

Wohl, E., Cenderelli, D. A., Dwire, K. A., Ryan-Burkett, S. E., Young, M. K., & Fausch, K. D. (2010). Large in-stream wood studies: A call for common metrics. *Earth Surface Processes and Landforms*, *35*, 618–625. https://doi.org/10.1002/esp.1966

Xu, Y., & Liu, X. (2016). 3D computational modeling of stream flow resistance due to large woody debris. In Constantinescu, Garcia & Hanes (Eds.), *Proceedings of River Flow 2016* (pp. 2346–2353). St. Louis, MO, ISBN 978-1-315-64447-9.

Yen, B. (2002). Open channel flow resistance. *Journal of Hydraulic Engineering*, *128*, 20–39.

SUPPORTING INFORMATION

Additional supporting information may be found online in the Supporting Information section at the end of this article.

How to cite this article: De Cicco PN, Paris E, Solari L, Ruiz-Villanueva V. Bridge pier shape influence on wood accumulation: Outcomes from flume experiments and numerical modelling. *J Flood Risk Management*. 2020;e12599. https://doi.org/10.1111/jfr3.12599